Single trapped ions interacting
with low- and high-finesse optical cavities

J. Eschner[*]**, Ch. Raab, A. Mundt, A. Kreuter, C. Becher, F. Schmidt-Kaler**, and **R. Blatt**

Universität Innsbruck, Institut für Experimentalphysik, Technikerstr. 25, 6020 Innsbruck, Austria

The presence of mirrors modifies both the coherent coupling of an atom to a light mode and its spontaneous emission into the mode [1]. We study such cavity QED effects experimentally with single ions and optical cavities. We focus on two examples which are equally interesting as fundamental systems and for application in quantum information processing. (i) By retroreflecting the fluorescence of a single trapped Ba^+ ion with a mirror 25 cm away, we observe inhibition and enhancement of the atom's spontaneous emission. When two ions are trapped, the distant mirror creates super- and subradiance. (ii) With a single trapped Ca^+ ion we demonstrate coherent coupling of its narrow $S_{1/2} - D_{5/2}$ "qubit" transition to a mode of a high-finesse optical cavity. We also achieve deterministic coupling of the cavity standing wave to the ion's vibrational state by controlling the ion's position with nanometer-precision and selectively exciting vibrational state-changing transitions.

1 Introduction

Since the first single ion was experimentally prepared and observed [2], single trapped atoms have found numerous applications. These range from frequency standards and precision measurements of physical constants [3] over experiments on fundamental quantum mechanics to their application for the storage and processing of quantum information. The lasting interest in single trapped ions is based on unique properties which become possible through the combination of a Paul type ion trap with laser cooling. These techniques result in a localization of the single particle to a few ten nanometers or below, in a control of the motional state down to the zero-point of the trapping potential, in a high degree of isolation of the ion from its environment, and in quasi unlimited interaction time.

During the last few years, experiments with single atoms have moved on towards coherent manipulation of their internal and motional quantum state, thus opening another rich field of applications: When applied to several ions in the same trap, such manipulations form the basis of an experimental implementation of quantum information processing [4]. Several important steps into this direction, such as the preparation of pure quantum states [5–7], their unitary rotation with high fidelity [6–8], conditional dynamics [8], as well as deterministic entanglement of a trapped ion string [9] have already been demonstrated.

Here we report on single-ion experiments which illustrate equally the field of fundamental studies with single trapped particles as well as their application for quantum information processing. In the first experiment [10], we investigate interference phenomena in the light emitted by single Barium ions when this light is back-reflected to interact again with the same ion or with another ion. We demonstrate that a single distant mirror ("a low-finesse cavity") creates inhibited and enhanced spontaneous emission of a single ion and sub- and superradiant emission of two ions, through free-space interaction over 50 cm distance.

In the second experiment [11], we couple a mode of a high-finesse optical cavity coherently to a narrow "qubit" transition in a single Calcium ion. The ion is excited by a short resonant pulse of the cavity

---

[*] Corresponding author   E-mail: juergen.eschner@uibk.ac.at
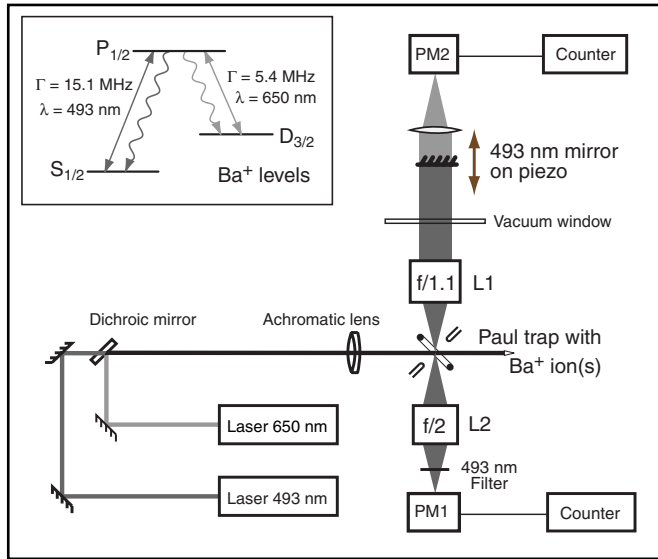
Fig. 1   Experimental setup and level diagram for Ba^+. See text for details.

field, and the resulting state of the qubit is read out by state-selective fluorescence. We also show that, by precisely positioning the ion in the standing wave of the cavity, the ion's quantized vibration in the trap is deterministically coupled to the cavity mode.

2   Low-finesse cavity

2.1   Experimental setup

The first experiment uses one or two single Ba^+ ion(s), trapped in a Paul trap of 1.4 mm diameter with axial (radial) oscillation frequencies between 1.2 and 2 (0.6 and 1) MHz. The ions are laser-cooled by continuous excitation on their $S_{1/2} \leftrightarrow P_{1/2}$ and $P_{1/2} \leftrightarrow D_{3/2}$ resonance lines at 493.4 nm and 649.7 nm, respectively. See Fig. 1 for a schematic of the experiment and the relevant levels of Ba^+; more details are described in earlier publications [12]. Both lasers have linewidths well below 100 kHz. The laser beams are combined on a dichroic beamsplitter before they are focused into the trap, and both light fields are linearly polarized. The laser intensities at the position of the ion are set roughly to saturation. The 650 nm laser is tuned close to resonance, the 493 nm laser is red-detuned by about the transition linewidth ($\Gamma = 15.1$ MHz) for Doppler cooling.

A high-quality lens (L1), oriented at $90°$ to the excitation beams and situated 12.5 mm away from the ion, collects the fluorescence light of the ion in 4% solid angle and transforms it into a parallel beam of 21.4 mm diameter. A mirror 25 cm away retroreflects the 493 nm part of the light collimated with L1, while transmitting the 650 nm part. The mirror is angle-tuned for $180°$ back-reflection with a precision mirror mount and, for fine adjustment, with two piezo translators (PZTs). The retroreflected light is focused by L1 to the position of the ion and, together with the light emitted directly into that direction, it is collected with a second lens (L2) at $-90°$ to the excitation beams and recorded with a photomultiplier (PM1). Coarse alignment, i.e. superposition of the ion and its mirror image, is controlled visually through L2 while fine adjustment is done by optimizing the signal. The distance between mirror and ion is varied by an amount d (in the range of $\pm 1\,\mu m$) by shifting the mirror along the optical axis with another PZT. The 650 nm light transmitted through the mirror is recorded by a second photomultiplier PM2.
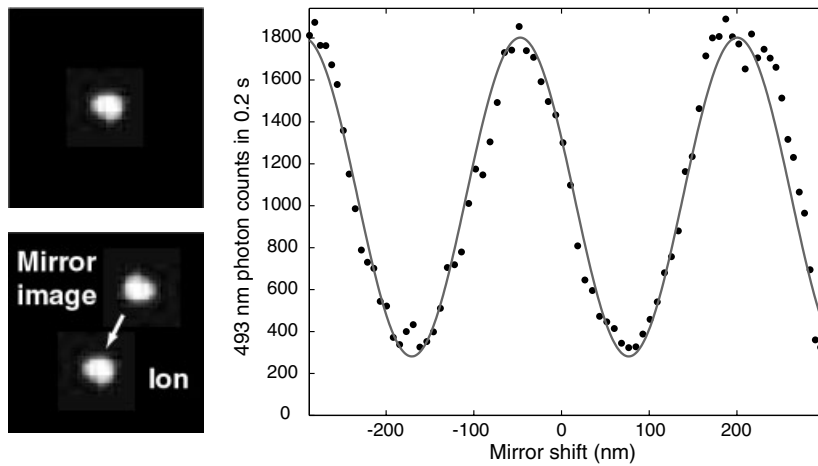
Fig. 2   Left: Photo of single ion (top) and schematic (bottom) illustrating the superposition of single ion and mirror image as seen through the observation channel (c.f. Fig. 1). Right: Interference of direct and back-reflected parts of the fluorescence of a single ion: Photon count rate at PM1 vs. mirror displacement (points). The fit (line) accounts for the nonlinear expansion of the PZT with applied voltage.

2.2   Results

2.2.1   One ion

Fig. 2 shows a scan of fluorescence vs. mirror shift when the direct and retroreflected part of the resonance fluorescence of a *single* Ba^+ ion are recorded together on PM1. Interference fringes appear which repeat when the mirror is shifted by half the 493 nm wavelength. The interference contrast (or visibility V) in this example is 72%; no background was subtracted from the data. We have identified various sources of visibility reduction: Residual thermal motion of the ion limits it to 86%, spectral broadening due to inelastic scattering reduces it by another 2%. The remaining reduction is caused by abberations in the optical system and acoustic noise.

The observation shows clearly that light from the ion and from its mirror image, i.e. light scattered by the same atom into opposite directions, is coherent and can therefore interfere. In other words, the two pathways of a scattered photon into the detector are indistinguishable. While such interference would also be observed if the two light fields were superimposed on a beam splitter, the particular feature of this experiment is that the two fields are superimposed at the position of the ion. Thereby, our retroreflecting lens-mirror setup creates a *back-action* on the atom which is a fundamentally different effect. In the language of cavity QED this back-action is explained by a modification of the electromagnetic vacuum at the position of the ion: The mirror creates nodes and antinodes in those modes which are collimated by the lens and then retroreflected, among them the modes which are analyzed by the detector. Since the spontaneous emission into any of these modes is proportional to the mode intensity at the position of the ion, we observe reduced or increased fluorescence depending on whether the ion is at a node or antinode, i.e. depending on its distance from the mirror.

If some fraction of the total fluorescence is suppressed or enhanced, we expect the total rate of fluorescence to vary at roughly the same percentage level. An observation of such a variation would verify that the described back-action takes place. Therefore we recorded, simultaneously with the interference fringes, the fluorescence at 650 nm which is transmitted through the mirror (see Fig. 1) and which is directly proportional to the population of the excited $P_{1/2}$ level of the ion. The result is shown in Fig. 3. The 650 nm fluorescence exhibits a clear $\sim 1\%$ sinusoidal variation anticorrelated with the interference signal, indicating that an
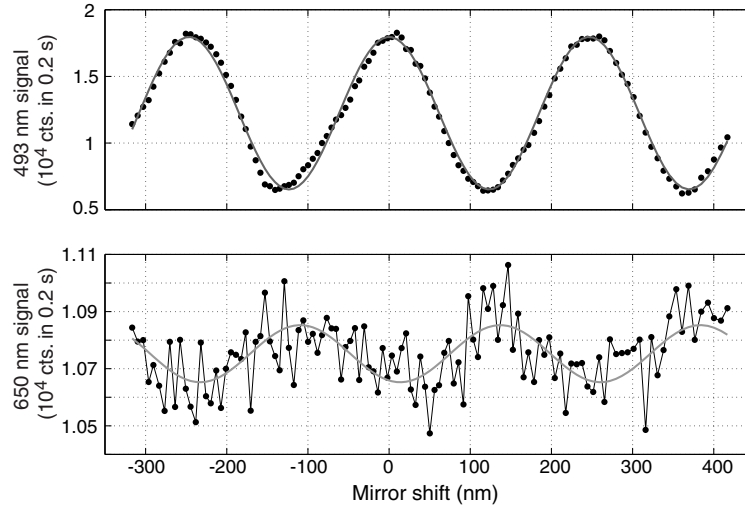
Fig. 3 Interference fringes at 493 nm, observed on PM1 (top), and simultaneously recorded fluorescence at 650 nm transmitted through the mirror and observed on PM2, (bottom). Points are experimental data, bold lines are fits showing sinusoidal oscillations at the same frequency. The visibility of the modulation is 47% (top) and 0.9% (bottom). The phase lag between the two oscillations is close to 180°, as expected from the simple physical picture (see Sect. 2.3). However, the small deviation from 180° is statistically significant and may be caused by an energy shift of the $P_{1/2}$ level due to the presence of the mirror [13].

interference minimum (maximum) at 493 nm leads to higher (lower) population of the excited state. This shows that the mirror 25 cm away in fact acts on the internal atomic dynamics of the ion.

2.2.2 Two ions

With the same setup as before but with *two* laser-cooled ions in the trap, we adjust the mirror such that the mirror image of each ion is superimposed with the real image of the other ion. When we scan the mirror we find a result as displayed in Fig. 4. Again, interference fringes appear with the same period as before and with about 5% contrast. However, their interpretation must be clearly different since it is not light from the same atom that interferes, neither is there a back-action of an atom on itself. Instead, the two indistinguishable processes which create the interference are emission by one ion towards the detector and emission by the
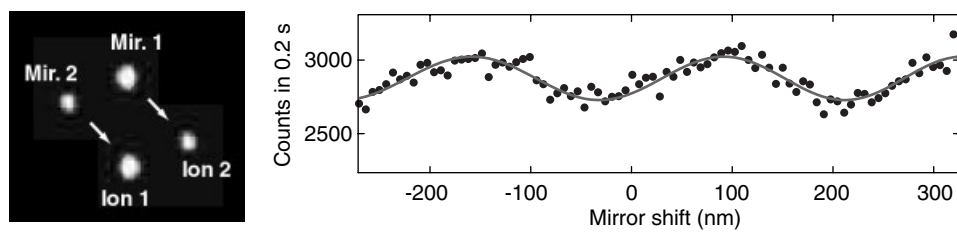

Fig. 4 Left: Schematic (based on photo of two ions in the trap) illustrating the superposition of ions and mirror images, as viewed through the observation channel. Right: Interference fringes as in Fig. 4 but now with two ions, each interfering with the mirror image of the other. The visibility is ∼ 5%; the main reason for its reduction, compared to the one-ion experiment, is the strong driven (micro-) motion of the ions in the Paul trap when their mutual repulsion displaces them from the trap center.

other towards the mirror, and, rather than back-acting onto themselves, the two atoms interact with each other by exchanging photons.

2.3   Model description

To include the back-action or interaction created by the mirror into the Optical Bloch Equations (OBEs) for the atomic dynamics we have to take into account that the two possible pathways for a photon to reach the detector are indistinguishable. In a phenomenological approach [10], this can be represented by adding coherently the two decay processes, one of them delayed by the travel time τ to the mirror and back. A corresponding calculation for the one-ion case, using the parameters of Fig. 2, indeed predicts a variation of the total fluorescence with the ion-mirror distance. The measured value of 0.9% visibility is found when the effective fraction of the total emitted light which can be brought to interference is set to 1.7%. This kind of variation of the total fluorescence rate due to mirrors or other dielectric boundary conditions is commonly called inhibited and enhanced spontaneous emission; it can also be regarded to result from reabsorption or stimulated emission induced by the back-reflected photons.

In an effort to model the situation in much more detail and generality, modified OBEs containing the memory effect created by the mirror have recently been derived and studied by Dorner et al. [13]. Regarding the contrast of the interference and its interpretation, they come to essentially the same conclusions. Moreover, they predict interesting additional effects, in particular that the mirror causes an energy shift of the excited level, which can be interpreted as a resonant Lamb-shift known from cavity QED experiments [14, 15]. This level shift may be responsible for the observed phase lag between the interference signal and the variation of the upper-state population which can be seen in Fig. 3.

To model the two-ion case in the same phenomenological fashion as the single ion, we modify the OBEs for the two-atom density matrix by adding coherently emission from ion 1 straight into the detector and emission from ion 2 towards the mirror, and vice versa. We find that a new term appears in the dynamics which describes simultaneous emission by one ion and absorption by the other and which is modulated with the distance between the ions via the mirror. This shows that in fact reabsorption (and its inhibition) of the emitted photons goes along with the observed interference in the two-ion case. A slightly different viewpoint is that, depending on the delay τ, either the symmetric or the antisymmetric two-atom wave function is preferentially populated, which leads to enhanced or suppressed collective spontaneous emission, respectively. This is sub- and superradiance as originally described by Dicke [16]. In an earlier experiment [17] the corresponding lifetime modification was studied with two ions whose spacing was reduced to about 1.5 μm by a strongly confining trap. In our case, their interaction is mediated by the lens-mirror system over a distance of 50 cm.

3   High-finesse cavity

3.1   Setup and measurement procedure

The setup of the second experiment is schematically shown in Fig. 5. The single Ca^+ ion in the 3-dimensional RF-Paul trap has secular frequencies $\omega_{x,y,z} = 2\pi \times (2.9, 3.9, 7.4)$ MHz. Here, z denotes the direction of the trap axis, which is at 45° to the cavity axis. The x and y radial directions both include an angle of $\approx 45°$ with the plane spanned by cavity and trap axis. The trap is placed in the center of a near-confocal resonator with mirror separation $L = 21$ mm, radius of curvature $R_M = 25$ mm, waist radius $\omega_0 = 54$ μm, and finesse $\mathcal{F} = 35000$ at 729 nm. Cylindrical piezoceramics (PZT) allow fine-tuning of the cavity length across approx. 1.5 free spectral ranges. Coherent coupling of the ion to the cavity field is measured in three steps:

(i) *Preparation*: First we apply Doppler cooling on the $S_{1/2} - P_{1/2}$ transition at 397 nm (see Fig. 5). A repumper laser at 866 nm inhibits optical pumping into the $D_{3/2}$ level. From the measured mean vibrational quantum numbers after Doppler cooling [11], $(\bar{n}_x, \bar{n}_y, \bar{n}_z) = (20 \pm 5, 4 \pm 1, 6 \pm 1)$, we calculate an rms
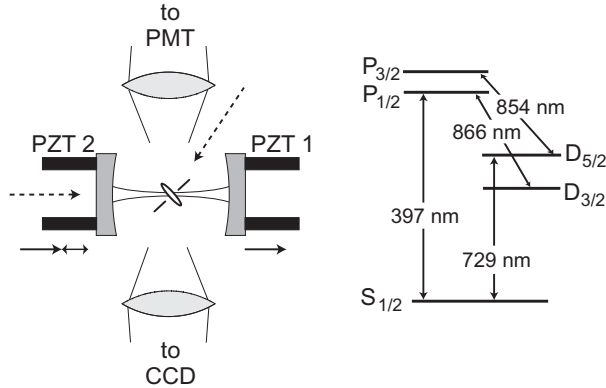
Fig. 5 Schematic experimental setup (left) and Ca$^+$ level scheme (right). PZT1 denotes the offset piezo, PZT2 the scan piezo (see text). A photomultiplier (PMT) records fluorescence on the $S_{1/2} - P_{1/2}$ transition and the CCD camera monitors the ion's position. The whole laser system is described in more detail elsewhere [19]. The dotted arrows indicate directions of laser beams: 729 nm laser along the cavity axis, 397 nm cooling laser, 854 nm and 866 nm auxiliary lasers at an angle to the trap axis.

extension of the ion's motional wave packet of 25 ± 5 nm along the cavity axis, much smaller than the wavelength of 729 nm (Lamb-Dicke regime). After cooling, the ion is prepared in the $S_{1/2}(m = -1/2)$ substate by optical pumping with σ^- radiation at 397 nm.

(ii) *Interaction*: The laser at 729 nm is set to a fixed detuning Δ from the $S_{1/2} - D_{5/2}$ ($m = -1/2$ to $m' = -5/2$) qubit transition. We inject the laser light into the TEM$_{00}$ mode of the cavity and scan the cavity with a voltage ramp applied to the scan PZT (PZT2). When the cavity reaches resonance with the laser frequency, it fills with light and the ion is excited. The scan rates used are such that the cavity is swept over its HWHM bandwidth ($2\pi \times 0.10$ MHz) in 2...6 cavity lifetimes of 0.78 μs. A constant voltage is applied to the offset PZT (PZT1) that determines the ion's position relative to the standing wave (SW) field.

(iii) *State analysis*: Resonant excitation on the $S_{1/2} - P_{1/2}$ dipole transition at 397 nm is used to discriminate between excited state (electron shelved in $D_{5/2}$, no fluorescence) and ground state (fluorescence). A short pulse of 854 nm light returns the ion to the ground state if it was found in the $D_{5/2}$ state. Note that although state detection happens about 1 ms after the cavity-ion interaction, the ion's state is well preserved due to the long lifetime (1 s) of the $D_{5/2}$ level.

In order to obtain an excitation spectrum, the 729 nm laser is tuned over the quadrupole transition in steps of about 1 kHz, and for any given laser detuning Δ the sequence (i)-(iii) is repeated 100 times to determine the excitation probability.

3.2 Results

3.2.1 Temporal variation of cavity field

First we placed the ion close to a node of the SW field [20] and probed its response to the temporal variation of the intracavity field. The sign of the voltage ramp applied to the scan PZT determines whether the scan mirror moves towards the offset mirror or away from it. For a negative (positive) scan rate, i.e. mirrors moving towards each other (apart), the intracavity field is Doppler blue (red) shifted and thus the excitation spectrum will be red (blue) shifted, as the excitation laser detuning has to compensate for the Doppler shift. Fig. 6 shows a result where the cavity scan rate was one HWHM bandwidth in 6 lifetimes. The excitation spectra show the expected blue shift (red shift) for increasing positive (negative) scan rates. The peak excitation probability of more than 0.5 clearly demonstrates that the ion is coherently interacting with the intracavity field.

We model the excitation for different laser detunings Δ by numerically integrating 2-level Bloch-equations using the time-dependent intracavity field calculated from the pertaining differential equations [21, 22]. The results of the simulation for positive scan rate is shown superimposed on the blue shifted spectrum in Fig. 6.
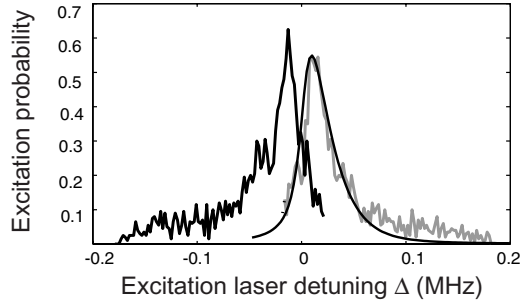
Fig. 6 Excitation spectrum of the $S_{1/2} - D_{5/2}$ transition. The blue shifted excitation spectrum is drawn in gray on the right hand side of the diagram, the superimposed solid line shows the theoretical simulation. The parameters used for the simulation are: excitation laser bandwidth $\Delta\nu_{Laser} = 6\,\text{kHz}$, natural linewidth of the $S_{1/2} - D_{5/2}$ transition $\Delta\nu_{SD} = 0.17\,\text{Hz}$, maximum Rabi frequency at the transition center wavelength $\Omega_{max} = 15.5\,\text{kHz}$, and the cavity parameters given in the text.
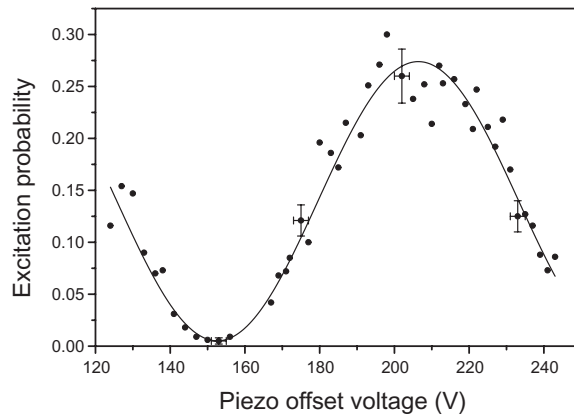

Fig. 7 Excitation probability on the $S_{1/2} - D_{5/2}$ transition as function of the PZT offset voltage, i.e. at various positions in the intracavity standing wave field. The solid line represents a $\sin^2$ function fitted to the data points. Error bars given for representative data points are due to PZT hysteresis (abscissa) and the errors of the fit (ordinate).

3.2.2 Spatial variation of cavity field

The second type of experiment probes the ion's response to spatial field variations. For this, we leave the scan rate at the same value as in Fig. 6. The intensity of the 729 nm laser is adjusted such that the excitation is kept well below saturation. The offset voltage of both scan PZT and offset PZT is then varied simultaneously in such a way that the SW in the cavity is shifted longitudinally with respect to the location of the ion. The position-dependent excitation probability is determined by fitting each excitation spectrum with a Lorentzian and adopting the peak value. Fig. 7 displays these values as function of the PZT offset voltage.

The excitation probability varies spatially with the intensity of the SW [20]. A theoretical Bloch-equation analysis, as described above, predicts a nearly pure $\sin^2$ spatial variation, deviating by less than 1%. From a $\sin^2$ fit to the data points we obtain $V = 96.3 \pm 2.6\%$ contrast ratio (visibility V) in the position-dependent excitation. This very high visibility results from the strong confinement of the ion's wavefunction. The laser-cooled ion, oscillating with its secular frequencies and with thermally distributed amplitudes, has an rms spatial extension along the cavity axis of a_c, which leads to a reduction of the excitation contrast by a factor $\exp(-2(2\pi a_c/\lambda)^2)$. From the measured visibility V we find $a_c = 16^{+5}_{-7}$ nm. This small value of the spatial extension shows that in this experiment we cool the ion close to the Doppler limit (13 nm).

A necessary condition for all experiments relying on ion-cavity mode coupling is the ability to place the ion at a certain position of the intracavity SW field with high precision and high reproducibility [23]. In our experiment, the precision of positioning the center of the ion's wavefunction, using a measurement as in Fig. 7, is limited by the uncertainty in the measured excitation probability. From the error bars in Fig. 7 we deduce a spatial precision between 7 nm ($\approx \lambda/100$) at the position of largest slope and 12 nm and 36 nm at minimum or maximum excitation, respectively. We note, however, that the precision can be enhanced by averaging over a larger number of state detection measurements.
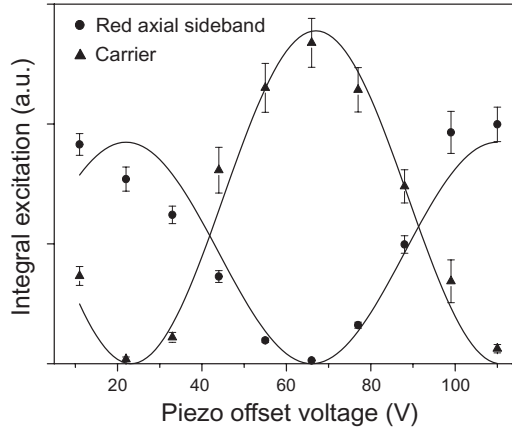
Fig. 8 Integral excitation on the carrier (triangles) and the red axial sideband (circles) of the $S_{1/2} - D_{5/2}$ transition as function of the PZT offset voltage, i.e. at various positions in the intracavity standing wave field. The solid lines represent fits of $\sin^2$ functions to the data points.

3.2.3 Coupling the quantum motion to the cavity field

Many schemes for quantum information processing with trapped ions rely on coherent interaction not only with the internal state but also with the motional degrees of freedom. A controlled coupling to the motional quantum state is a precondition for realizing such schemes. We recorded excitation probabilities of the ion at a fixed cavity scan rate (slightly larger than before), for different positions within the SW, and with the laser at 729 nm now tuned to either the carrier (no change of vibrational quantum number, $\Delta n = 0$) or the red axial sideband (laser detuned by $-\omega_z$, $\Delta n = -1$) of the $S_{1/2} - D_{5/2}$ transition. In both cases, the intensity of the laser was adjusted such that the excitations of carrier and sideband were comparable and were kept well below saturation. In this experiment we determined the integral excitation, i.e. the area of the respective excitation spectra, as the spectra show an asymmetric line shape [11].

As displayed in Fig. 8, carrier and sideband excitations both map the SW spatial field variation, but the traces are shifted by a phase factor of π. This phase shift arises due to symmetry characteristics of the transition matrix elements of carrier and sideband transitions in a SW field [24, 25]: The spatial part of the quadrupole transition matrix element is proportional to $\langle n'| \exp(ikx)|n\rangle$ for a travelling wave (TW) and $\langle n'| \cos(kx)|n\rangle$ for a SW with electric field $E \propto \sin(kx)$ [20]. Here n and n' are the vibrational quantum numbers in the $S_{1/2}$ and $D_{5/2}$ level, respectively, k is the wavenumber and x is the ion's position in the field. For a TW, all vibrational states (n, n') can be coupled as $\exp(ikx)$ contains even and odd powers of kx. In contrary, for a SW $\langle n'| \cos(kx)|n\rangle$ has to be expanded into even *or* odd powers of kx depending on the ion's position, e.g. $x = 0$ close to a node or $x = \lambda/4$ close to an anti-node. Thus, transitions changing the phonon number by even or odd integers are excited differently at different positions in the SW. The red sideband transition ($\Delta n = -1$) couples maximally at anti-nodes of the SW, whereas the carrier transition ($\Delta n = 0$) couples maximally at nodes.

The high-contrast orthogonal coupling of carrier and sideband transitions to the cavity mode enables applications such as cavity-assisted cooling [24] and entangling motional and photonic states when coupling to the cavity vacuum field [26, 27]. In particular, cavity-assisted cooling in a SW field means that sideband-cooling [6] on a red detuned vibrational sideband is facilitated by suppression of off-resonant carrier transitions which induce motional heating. In a similar fashion, unwanted off-resonant carrier excitations are suppressed when a cavity is used to drive sideband transitions in the Cirac-Zoller quantum-computing scheme [4]. This is interesting for applications since off-resonant carrier excitations impose a limit on the attainable gate speed [28].

4 Conclusions

We have studied cavity QED effects in two experimental systems. The origin of the phenomena is the same in both cases, a modification of the dielectric environment by mirrors. In the first experiment a distant mirror leads to a modification of the emission properties of a single ion and to a free-space coupling of two ions over ~ 50 cm distance. The experiment highlights particularly the intimate relation between the phenomena of inhibited and enhanced spontaneous emission of one ion and of sub-and superradiant emission of two ions. In the second experiment the coupling of a high-finesse optical cavity mode to a narrow "qubit" transition in a single ion is studied. We find coherent cavity-ion interaction when the cavity mode is excited with resonant light. We also showed that by placing the ion into either nodes or anti-nodes of the standing wave in the cavity and by setting the laser to either the carrier or the sideband frequency of the qubit transition, we can deterministically couple the cavity mode to the quantum motion of the ion.

Both experiments have in common that the strong confinement in the trapping potential leads to a localisation of the ion to a region much smaller than the optical wavelength, which is a prerequisite for the observed effects. Such atom-light coupling on sub-wavelength scales has recently been called "atomic nanoscope" [23]. In our first experiment, the ion's wavefunction extends over ~ 40 nm, in the second it is spread over only ~ 6 nm. This allows for the high contrast with which the ion couples to nodes and anti-nodes of the standing wave light field, marked by the visibility of the interference fringes in the first experiment, and by the contrast in the qubit excitation probability in the second. With even higher precision, the ion can be positioned within the standing wave: In the first experiment, fringe visibility and signal-to-noise ratio result in a positioning accuracy below 2 nm [10] in 0.2 s measurement time. The positioning accuracy for the ion in the cavity is ~ 7 nm; it can be easily improved by using a larger number of state measurements.

The experiments have various potential applications. Apart from its relevance as a demonstration of fundamental quantum phenomena at the single-atom level, the first setup can be extended towards free-space coupling of two individual atoms over long distances. It can also be used to generate entanglement between two separated atoms just by their optical interaction [29, 30]. Since the electronic quadrupole transition in Ca^+ is one of the candidates for implementing a quantum bit, the second experiment is a step towards realization of quantum computing and communication schemes with trapped ions that require a controlled interaction of ion and cavity field. Future experiments might extend the current configuration towards trapping of two or more ions coupled to a common cavity mode, thus allowing for implementation of quantum logical gate operations.

References

[1] E. M. Purcell, Phys. Rev. **69**, 681 (1946).
P. W. Milonni, The Quantum Vacuum (Academic, San Diego, 1994), in particular chap. 6.
K. H. Drexhage, in: Progress in Optics Vol. 12, pp. 163–232, edited by E. Wolf (North-Holland, Amsterdam 1974).
F. DeMartini, G. Innocenti, G. R. Jacobovitz, and P. Mataloni, Phys. Rev. Lett. **59**, 2955–2958 (1987).
W. Jhe, A. Anderson, E. A. Hinds, D. Meschede, L. Moi, and S. Haroche, Phys. Rev. Lett. **58**, 666–669 (1987).
D. J. Heinzen, J. J. Childs, J. F. Thomas, and M. S. Feld, Phys. Rev. Lett. **58**, 1320–1323 (1987).
C. J. Hood, T. W. Lynn, A. C. Doherty, A. S. Parkins, and H. J. Kimble, Science **287**, 1447–1453 (2000).
P. W. H. Pinkse, T. Fischer, P. Maunz, and G. Rempe, Nature **404**, 365–368 (2000).

P. Goy, J. M. Raimond, M. Gross, and S. Haroche, Phys. Rev. Lett. **50**, 1903–1906 (1983).

R. G. Hulet, E. S. Hilfer, and D. Kleppner, Phys. Rev. Lett. **55**, 2137–2140 (1985).

G. Rempe, H. Walther, and N. Klein, Phys. Rev. Lett. **58**, 353–356 (1987).

G. Gabrielse and H. G. Dehmelt, Phys. Rev. Lett. **55**, 67–70 (1985).

[2] W. Neuhauser, M. Hohenstatt, P. Toschek, and H. Dehmelt, Phys. Rev. A **22**, 1137–1140 (1980).

[3] R. J. Rafac, B. C. Young, J. A. Beall, W. M. Itano, D. J. Wineland, and J. C. Bergquist, Phys. Rev. Lett. **85**, 2462–2465 (2000).

[4] J. I. Cirac and P. Zoller, Phys. Rev. Lett. **74** 4091–4094 (1995).

[5] F. Diedrich, J. C. Bergquist, W. M. Itano, and D. J. Wineland, Phys. Rev. Lett. **62**, 403–406 (1989).

C. Monroe, D. M. Meekhof, B. E. King, S. R. Jefferts, W. M. Itano, D. J. Wineland, and P. Gould, Phys. Rev. Lett. **75**, 4011–4014 (1995).

B. E. King, C. S. Wood, C. J. Myatt, Q. A. Turchette, D. Leibfried, W. M. Itano, C. Monroe, and D. J. Wineland, Phys. Rev. Lett. **81**, 1525–1528 (1998).

[6] Ch. Roos, Th. Zeiger, H. Rohde, H. C. Nägerl, J. Eschner, D. Leibfried, F. Schmidt-Kaler, and R. Blatt, Phys. Rev. Lett. **83**, 4713–4716 (1999).

[7] H. Rohde, S. T. Gulde, C. F. Roos, P. A. Barton, D. Leibfried, J. Eschner, F. Schmidt-Kaler, and R. Blatt, J. Opt. B, Quantum Semiclassical Opt. **3**, S34-S41 (2001).

[8] C. Monroe, D. M. Meekhof, B. E. King, W. M. Itano, and D. J. Wineland, Phys. Rev. Lett. **75**, 4714–4717 (1995).

[9] C. A. Sackett, D. Kielpinski, B. E. King, C. Langer, V. Meyer, C. J. Myatt, M. Rowe, Q. A. Turchette, W. M. Itano, D. J. Wineland, and C. Monroe, Nature **404**, 256–259 (2000).

[10] J. Eschner, C. Raab, F. Schmidt-Kaler, and R. Blatt, Nature **413**, 495–498 (2001).

[11] A. B. Mundt, A. Kreuter, C. Becher, D. Leibfried, J. Eschner, F. Schmidt-Kaler, and R. Blatt, quant-ph/0202112.

[12] C. Raab, J. Bolle, H. Oberst, J. Eschner, F. Schmidt-Kaler, and R. Blatt, Appl. Phys. B **67**, 683–688 (1998); Appl. Phys. B **69**, 253 (1999); Phys. Rev. Lett. **85**, 538–541 (2000).

[13] U. Dorner and P. Zoller, quant-ph/0203147 (2002).

[14] M. Brune, F. Schmidt-Kaler, A. Maali, J. Dreyer, E. Hagley, J. M. Raimond, and S. Haroche, Phys. Rev. Lett. **76**, 1800–1803 (1996).

[15] D. J. Heinzen and M. S. Feld, Phys. Rev. Lett. **59**, 2623–2626 (1987).

[16] R. H. Dicke, Phys. Rev. **93**, 99–110 (1954).

[17] R. G. DeVoe and R. G. Brewer, Phys. Rev. Lett. **76**, 2049–2052 (1996).

[18] S. Gulde, D. Rotter, P. Barton, F. Schmidt-Kaler, R. Blatt, and W. Hogervorst, Appl. Phys. B **73**, 861 (2001).

[19] H.C. Nägerl, Ch. Roos, D. Leibfried, H. Rohde, G. Thalhammer, J. Eschner, F. Schmidt-Kaler, and R. Blatt, Phys. Rev. A **61**, 023405 (2000).

[20] Note that the atomic quadrupole moment couples to the gradient of the electric field. The maximum excitation thus occurs at the nodes of the standing wave.

[21] H. Rohde, J. Eschner, F. Schmidt-Kaler, and R. Blatt, J. Opt. Soc. Am. B, Opt. Phys. **19**, 1425–1429 (2002); physics/0107038.

[22] M. J. Lawrence, B. Willke, M. E. Husman, E. K. Gustafson, and R. L. Byer, J. Opt. Soc. Am. B, Opt. Phys. **16**, 523 (1999).

[23] G. R. Guthöhrlein, M. Keller, W. Lange, H. Walther, and K. Hayasaka, Nature **414**, 49–51 (2001).

[24] J. I. Cirac, R. Blatt, P. Zoller, and W. D. Phillips, Phys. Rev. A **46**, 2668 (1992).

[25] M. Šašura and V. Bužek, quant-ph/0112041.

[26] V. Bužek, G. Drobný, M. S. Kim, G. Adam, and P. L. Knight, Phys. Rev. A **56**, 2352 (1997).

[27] F. L. Semião, A. Vidiella-Barranco, and J. A. Roversi, Phys. Rev. A **64**, 024305 (2001).

[28] A. Steane, C. F. Roos, D. Stevens, A. Mundt, D. Leibfried, F. Schmidt-Kaler, and R. Blatt, Phys. Rev. A **62**, 042305 (2000).

[29] D. Braun, quant-ph/0205019.

[30] C. Cabrillo, J. I. Cirac, P. Garcia-Fernandez, and P. Zoller, Phys. Rev. A **59**, 1025 (1999).